Joule heating of carbon fibre tapes – A low-cost approach for automated dry fibre deposition

Shimin Lu[1], Peihao Song[2], Lee Harper[1]*, Thomas Turner[1]

1. Composites Research Group, University of Nottingham, Nottingham, NG7 2RD, UK
2. Department of Engineering Science, University of Oxford, Parks Road, OX1 3PJ, UK

*Corresponding author – lee.harper@nottingham.ac.uk

Abstract

Joule heating is potentially a low-cost option for activating the binder on the surface of carbon fibre tapes during automated dry fibre placement (ADFP). In this paper, the electrical contact resistance between a carbon fibre tape and cylindrical electrodes is characterised experimentally using a tabletop rig to replicate the process conditions encountered during ADFP. This rig is used to study a range of wrap angles, fibre tensions and temperatures to inform the design of a Joule heating setup for a lab-scale ADFP fibre deposition rig. A validated model has been developed to predict the tape temperature at the nip point for different current inputs and deposition velocities. Increasing both fibre tension and wrap angle are found to reduce contact resistance and increase heating efficiency. A nip point temperature of 200 °C can be achieved by Joule heating for a single carbon fibre tape at a deposition velocity of 100 mm/s, using a power of 110 W. This equates to a 17% reduction in energy compared to laser heating.

Keywords

Dry tape, electrical contact resistance, Joule heating, automated fibre placement (AFP)

1 Introduction

Automated deposition processes for fibre reinforcement, such as automated tape laying (ATL) and automated fibre placement (AFP), have been used in the composites industry for several decades since they enable higher layup speeds, improve accuracy and reproducibility, reduce waste, and reduce labour costs over hand layup processes [1]. Prepreg materials are commonly used in these processes, but there has been an impetus to move to using bindered dry fibre tapes to reduce material costs. Automated dry fibre placement (ADFP) is used to produce preforms for out-of-autoclave processes such as

liquid resin infusion, potentially requiring less machine downtime for repair over conventional prepreg-based AFP machines [2].

The binder on the surface of the tapes requires thermal activation at relatively high temperatures (>160 °C), therefore laser heating is commonly used to achieve the rapid heating rates (>300 °C/s) required for high rate tape deposition [1-5]. Laser heating methods create health and safety concerns [1], therefore hot gas torches are another common heating method applied to ADFP [6] but temperatures can be more difficult to control [7]. Flashlamp heating has also been used in ADFP [8, 9], such as the Humm3® heating system by Heraeus, but it typically consumes more energy than laser heating to achieve the same material temperature [8].

Joule heating is a possibility since the stabilised dry carbon fibre tapes have no bulk matrix material on the surface to affect the electrical conductivity. Joule heating, also known as resistive or ohmic heating, is the phenomenon whereby the passage of electrical current through a conductive medium produces heat. First published in 1840, Joule's first law states that the power absorbed by this process is equal to the product of the conductor's resistance and the square of the current flowing [10]. This is an efficient heating mechanism with direct conversion of electrical power into heat, which has found applications in many resistive heating elements such as in domestic kettles or ovens. The relatively low resistivity of carbon fibres enables them to conduct significant electrical current and therefore generate an increase in temperature due to the Joule effect. Joule heating has been used in the composites industry for curing thermoset composites [11, 12], resistance welding of thermoplastic composites [13, 14], on towpregging lines [15, 16] and for de-icing applications [17, 18]. Compared with alternative heating methods for ADFP, Joule heating is much simpler and cheaper to set up and there are fewer safety concerns [19], however, there is a lack of understanding about the interaction between carbon fibres and the heating hardware.

Good electrical contact between the carbon fibres and the electrodes is critical when applying Joule heating to ADFP. Cylindrical rollers are normally used to facilitate smooth feeding of the carbon fibre tapes within the deposition head. Theses rollers can function as electrodes in Joule heating setup. Contact between the electrodes and the fibres is imperfect and an electrical contact resistance exists, leading to additional heat being generated in the contact region when a current is applied [16]. If this is not managed correctly, this additional contact resistance can cause hot spots and can burn the binder

system [20]. According to some published works, this contact resistance can be reduced by increasing the fibre tension [16], increasing contact pressure between the carbon fibres and the electrode and using a more compliant electrode, such as a conductive silicone roller [20].

Grohmann [21] successfully produced ADFP preforms using Joule heating. Subsequent composites were manufactured by resin infusion and it was found that the interlaminar shear strength for samples produced using Joule heating showed no differences to samples produced by infrared heating. Further work [19] investigated the contact resistance for a range of different tapes when in contact with the electrodes, using microscopy on the surface of the tapes to identify the binder coverage. Joule heating was considered to be a suitable heating method if there were sufficient uninsulated fibres visible and the overall contact resistance of the tape was low [19].

For AFP and ADFP, the nip point temperature beneath the deposition roller is an important process parameter controlling preform consolidation and consequently the final quality of manufactured parts. It is therefore important to understand the relationship between power input and temperature when applying Joule heating. Athanasopoulos *et al* [22] investigated Joule heating of stationary carbon fibre tows held under vacuum, both experimentally and numerically. Temperature dependent properties such as electrical resistance and specific heat capacity were employed in a model for the carbon fibre tows, enabling numerical predictions for the tow temperature to be within 5 °C of the setpoint (up to 300 °C) compared to experimental data. Grohmann [23] also developed a Joule heating model for stationary ADFP tapes using experimentally determined electrical resistance and specific heat capacity values. The model over predicted the tape temperature by 30 % compared to the experimental results, due to suspected inaccuracies in the measurement of the specific heat capacity. Çelik *et al* [15] built a finite element Joule heating model for a towpregging line, where carbon fibre tows were heated dynamically. Temperature independent material properties were used, but the prediction showed reasonable agreement (within 18%) with the experimental tow temperature across the range of values studied (from 50 to 120 °C). It was confirmed that the contact resistance heating is significant at the beginning of the heating region (around 50 °C at a current input of 2 A), therefore it is important to include this contribution within the model. Whilst Joule heating for the towpregging line example follows a similar principle to an ADFP head, the required

temperature set point is lower and there is no cooling effect from contact with the deposition roller compared to the current setup. No published work has been found on the relationship between temperature and power for Joule heating of carbon fibre tapes using an ADFP setup.

A tabletop rig has been built in this paper to characterise the contact resistance between two different carbon fibre tapes and a pair of cylindrical copper electrodes. The tapes are placed under different levels of tension, with different wrap angles at the contact points with the electrodes. The temperature dependent electrical resistance of the carbon fibre tapes and the relationship between the input current and steady-state heating temperature are also characterised using this rig. A Joule heating setup has subsequently been implemented on a lab-scale ADFP deposition rig, using a copper roller and a conductive tool as the electrodes. Deposition trials under different current inputs and deposition velocities have been conducted. A Joule heating model has been developed to predict the nip point heating temperature during ADFP deposition.

2 Experimental Approach

2.1 Materials

The primary material used in this study is a unidirectional consolidated tape (Solvay TX1100) with a nominal width of 6.35 mm. A 12K virgin carbon fibre tow (Toray 12 K T700-50C) is also used for experiments involving the tabletop Joule heating rig for comparison. Both carbon fibre materials are sized with an epoxy compatible sizing agent. The Solvay ADFP material has binder applied to one side and a non-woven veil over the other side to enhance infusion characteristics. Some details of the tape structure are given in the papers by Liu *et al* [4] and Veldenz *et al* [24]. In the current study, the bindered surface of the TX1100 tapes is placed in contact with the electrodes, since the electrical conductivity is higher than the veiled surface [19].

2.2 Material Characterisation

2.2.1 Specific heat capacity

The specific heat capacity of the carbon fibre tapes was established using a modulated differential scanning calorimeter (MDSC) using a DSC Q2000 from TA Instruments. Temperatures ranged from 30 °C to 250 °C, using a ramp rate of 2 °C/min. The modulation period was 60 s and the modulation amplitude was ± 1 °C. The sample

weight was around 9 mg. Linear regression was used to establish the specific heat capacity as a function of temperature for the two materials introduced above, as shown in Figure 1. The grade of carbon fibre used for the TX1100 tape (IMS65) is different to the T700 tow, plus the TX1100 contains binder and a surface veil, which both contribute to the difference in specific heat capacity.

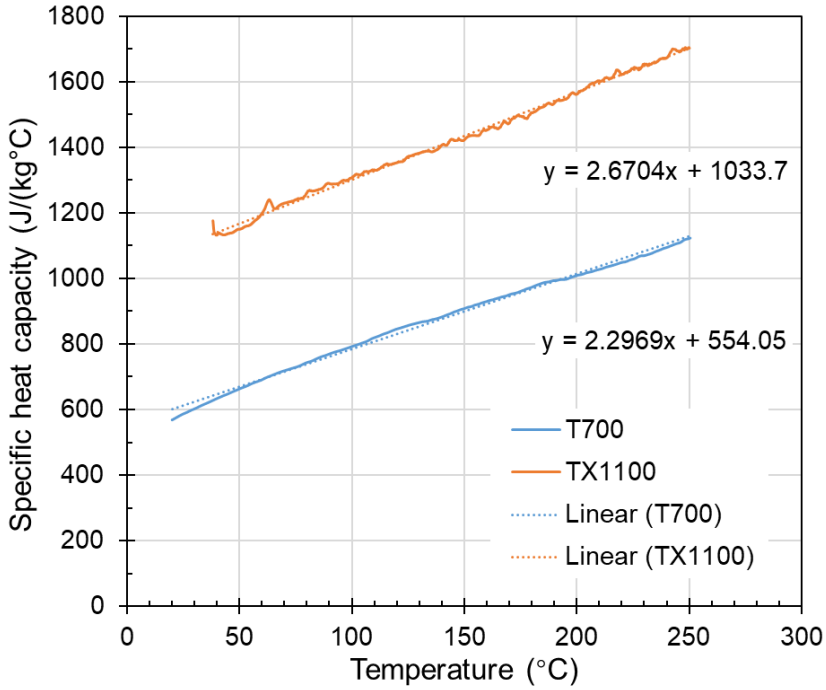

Figure 1 Temperature dependent specific heat capacity of T700 tows and TX1100 tapes

2.2.2 Electrical resistance and contact resistance

The procedure used by Çelik et al [16] was applied to measure the contact resistance between the carbon fibre tapes and the copper electrodes. A Joule heating tabletop test rig was developed to measure the contact resistance, as shown in Figure 2. The rig consists of two copper electrode tubes with a diameter of 22 mm and a guide tube. The distance between the two electrode tubes can be changed. A digital multimeter (KEITHLEY 2110) was used to measure the electrical resistance between the two tubes shown in Figure 2, using a four-wire arrangement with a measurement error of ±0.04 %. The total electrical resistance measured by the multimeter is the sum of the contact resistance of the two contact regions, the carbon fibre tape resistance and copper electrodes resistance. The electrical resistance of the copper electrodes is considered to be negligible. The total resistance was measured for four different tape lengths (50 mm, 100 mm, 150 mm and 200 mm) between the two electrodes. The electrical resistance

of the carbon fibre tape increases linearly with increasing tape length. When the total resistance values are plotted against length, the data points produce a linear trend and the intercept on the resistance axis can be used to determine the contact resistance. The slope of the fitted line is the electrical resistance per unit length of the carbon fibre tape. Figure 3 presents an example of contact resistance and electrical resistance measurement. In this case, the intercept is the contact resistance (1.80 Ω) while the slope is the specific resistance (21.75 Ω/m). The influence of fibre tension and wrap angle on the contact resistance can also be investigated using this rig. Fibre tension is applied by hanging a weight (from 100 g to 700 g) at one end of the carbon fibre tape. The wrap angle on the right electrode (Figure 2) where tension is applied is constant at 90°, but the wrap angle on the left electrode is changed by adjusting the position of the guide tube. Four wrap angles (31.0°, 42.7°, 82.4° and 116.1°) can be obtained.

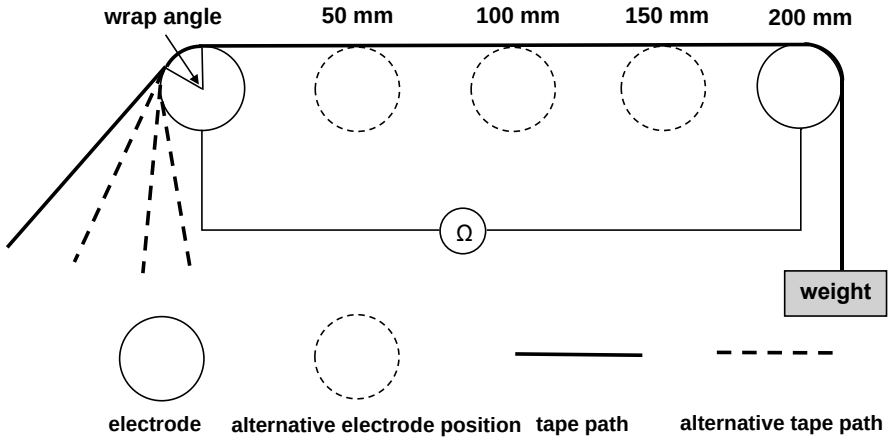

(a)

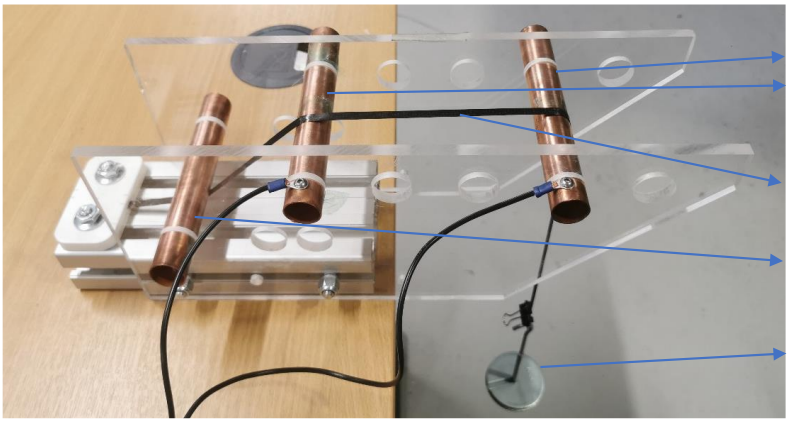

(b)

Figure 2 (a) Schematic of Joule heating rig (b) Photo of Joule heating rig. (The copper tubes on the top are used to change the heating length. The guiding tube on the bottom is used to change wrap angle. Two wires on the top copper tubes are connected to a multimeter to measure total resistance, or a power supply to provide heating.)

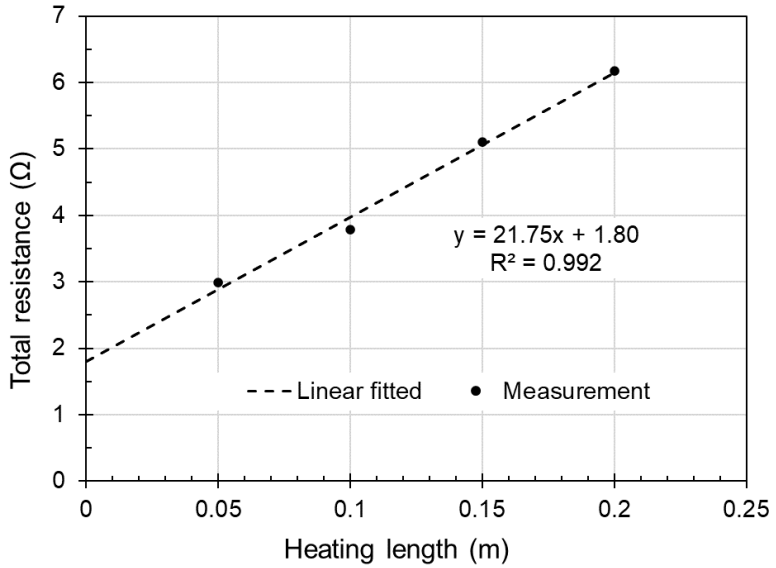

Figure 3 An example of contact resistance and specific electrical resistance measurement

2.2.3 Joule heating – Tabletop rig

Electrical currents pass though the Joule heating rig to heat the carbon fibre tapes, as shown in Figure 2. A power supply (Velleman LABPS3010SM) was used to provide constant voltage to the circuit. A shunt resistor (PCN RXM50) with an electrical resistance of 0.1 Ω was used for the current measurement. A Beckhoff EL3164 analogue input terminal was used to measure the voltage across the shunt resistor. The current in the circuit was obtained from the Beckhoff terminal voltage values divided by the shunt resistor's electrical resistance of 0.1 Ω. The digital multimeter was used to measure the voltage between the two wires of the Joule heating rig. The total resistance between the two wires in the Joule heating rig was then obtained from the multimeter voltage value divided by the circuit current value. Fibre tension and wrap angle were applied using the same method as the electrical resistance measurement experiments.

The carbon fibre tapes were heated up to a steady-state temperature and then the circuit current and multimeter voltage values were recorded. A FLIR thermal camera was used to measure the temperature of the carbon fibre tape.

Figure 4 shows a thermal image from the camera, demonstrating that the edges of the tape exhibit lower temperatures than the central region. These edge effects account for less than 20 % of the total surface area. The average temperature along the centreline has been compared to the average temperature from the rectangular region that covers 80% of the tow surface. The error between these measurements is less than 3%. The average temperature along the tape centre line has therefore been used to represent

the overall surface temperature of the tape, as shown in Figure 4. Three repeat measurements were conducted for each test.

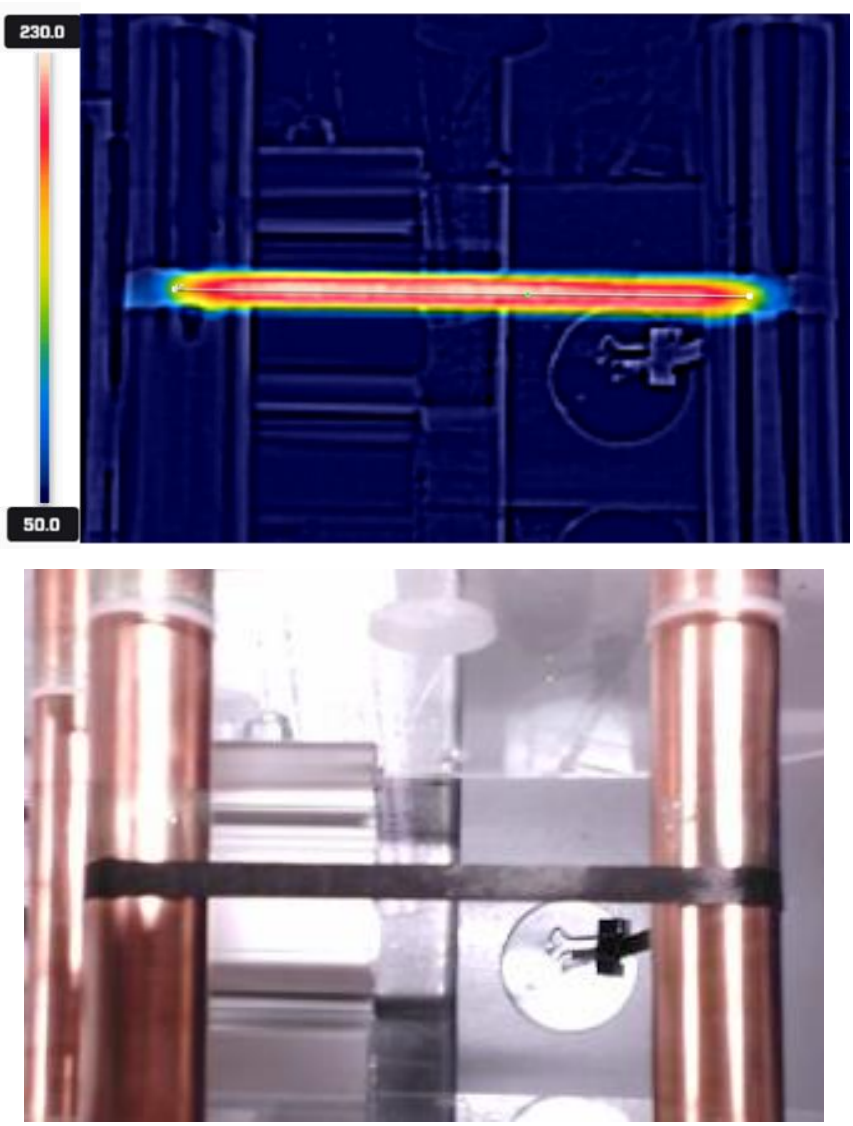

Figure 4 Temperature measurement of Joule heating in test rig (Average temperature along the centre line at steady-state is recorded.)

Using this Joule heating setup, the contact resistances between the carbon fibre tapes and the copper electrodes, plus the electrical resistance of the carbon fibre tapes at different temperature, were characterised. Tapes were heated to temperatures ranging between 30 °C and 200 °C for the four different lengths, enabling the total resistance to be recorded for each scenario. Linear interpolation was used to determine the total resistance as a function of tape heating temperature.

A stepped power input was used to conduct heating trials with the tabletop rig to validate the analytical model described in Section 3. The power was turned on for 30 seconds and then turned off. The measured current values from the shunt resistor were

used as the input for the analytical model to generate a heating and cooling curve. A FLIR thermal camera was used to continuously record the surface temperature in the centre of the tape.

2.2.4 Joule heating - ADFP deposition head

Joule heating tests were also conducted using a lab-scale ADFP deposition head, as shown in Figure 5. The carbon fibre tapes were heated between a copper roller electrode and a conductive substrate. Both electrodes made contact with a compaction roller, which was covered by a rubber skin with a Shore A hardness of 60 HA. The cylindrical copper electrode was forced to make contact with the deposition roller by a pneumatic cylinder. The conductive substrate (ADFP machine bed) was compacted by the deposition roller under a controlled force. The copper electrode roller was connected to the circuit via a carbon brush. A power supply (Velleman LABPS3010SM) was used to provide a constant current to the circuit. A shunt resistor (PCN RXM50) with an electrical resistance of 0.1 Ω was connected for the current measurement. Only one tape was deposited in each experiment. A FLIR thermal camera was mounted on the frame of the ADFP deposition head and was used to measure the average tape temperature in the region between the copper electrode and the nip point. The temperature along the fibre direction in this region was non-constant, since the section of tape near to the nip point experienced a longer heating time. Therefore, a small area perpendicular to the fibre direction was chosen to determine the average temperature, using a defined distance of 15 mm from the copper electrode (see Figure 6), since the nip point could not be directly visualised. The size of the measurement region was maximised, whilst ensuring it did not go beyond the edges of the tape.

Static Joule heating tests were initially performed on stationary tapes to characterise the heat loss caused by the thermal conduction between tapes and the deposition roller. Dynamic Joule heating tests were then performed during fibre deposition, using up to five different current values for each of the four deposition velocities, these values were chosen to yield similar heating temperature range. All test parameters are summarised in Table 1. Two repeats were conducted for each run. The deposition length was 800 mm and the temperature over the central 500 mm of tape was recorded to avoid the

acceleration/deceleration region of the machine. The compaction force for all tests was 30 N.

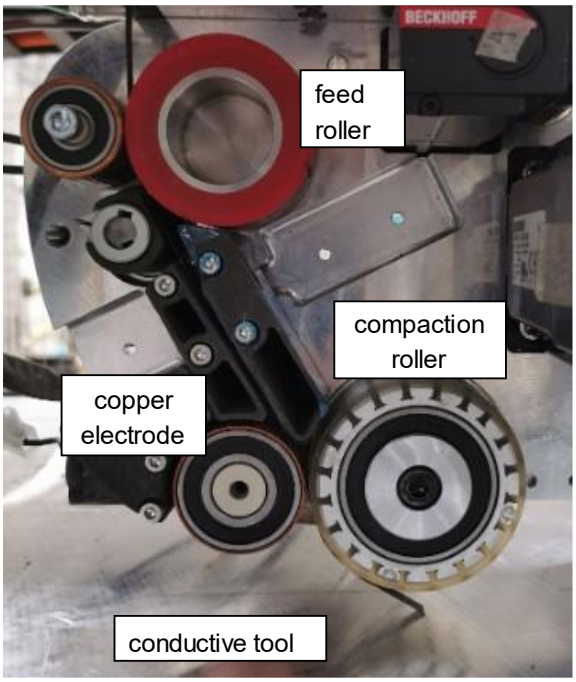

Figure 5 Deposition head of lab-scale ADFP rig: Joule heating of carbon fibre tapes between the copper electrode and the conductive tool.

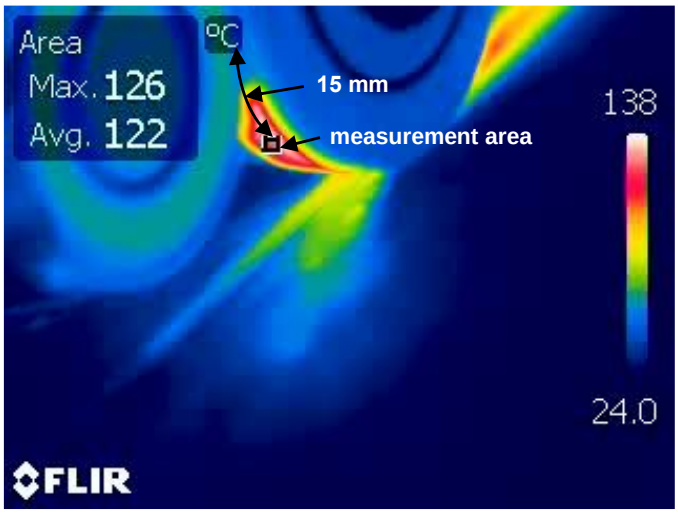

Figure 6 Temperature measurement of ADFP deposition using a FLIR thermal camera (measurement area is 15 mm after the copper electrode)

Table 1 Parameters used for heating with deposition tests

Test number	Current (A)	Deposition velocity (mm/s)
1	1.45, 1.97, 2.26	0
2-5	2.33, 2.55, 2.69, 3.11	10
6-10	2.82, 2.95, 3.21, 3.46, 3.66	25
11-14	3.21, 3.46, 4.02, 4.36	50
15-18	4.08, 4.36, 4.82, 5.14	100

3 Analytical Modelling

The goal of the modelling work is to predict the nip point Joule heating temperature. The transient heat transfer during the ADFP deposition process is complex, consisting of many components. These include contact resistance heating, Joule heating, convection cooling, radiation cooling, heat loss from the compaction roller and the movement of the carbon fibre tape. The model is developed incrementally, starting with a simple state-steady Joule heating model with carbon fibre tape exposed to air, where Joule heating, convective cooling and radiative cooling terms are included. Transient terms are then added to simulate the temperature history of the carbon fibre tape during Joule heating, accounting for heat loss to the ADFP deposition roller. Finally, a Joule heating model is established for the deposition of a carbon fibre tape using the ADFP head on the laboratory scale machine, using the parameters validated in the previous models.

3.1 Joule heating efficiency

The two contact resistances and the fibre resistance are electrically connected in series. The current passing through them is the same and is represented as I. The power used to heat the contact area P_c and the section of carbon fibre tape P_f can be calculated from Equation (1) and (2) based on Joule's law. $R_{c(T)}$ is the temperature dependent total contact resistance and $R_{f(T)}$ is the fibre tape resistance, which are both determined experimentally. The power efficiency of the Joule heating method, E, can then be calculated from Equation (3).

$$P_c = I^2 R_{c(T)} \quad (1)$$

$$P_f = I^2 R_{f(T)} \quad (2)$$

$$E = \frac{P_f}{P_f + P_c} = \frac{I^2 R_{f(T)}(T)}{I^2 R_{c(T)} + I^2 R_{f(T)}} = \frac{R_{f(T)}}{R_{f(T)} + R_{c(T)}} \quad (3)$$

3.2 Static steady-state Joule heating model

The carbon fibre tape is modelled as a rectangular solid block. A 1D heat transfer model is used to predict the Joule heating temperature along the fibre direction. The lower heating temperature at the tape edges as indicated in Figure 4, and the temperature gradient through the thickness direction cannot be accounted for in this model. The carbon fibre tape is exposed to air with Joule heating. When a steady-state is reached, the Joule heating input power is equal to the power losses from both radiative and convective cooling. This can be expressed by Equation (4) according to heat transfer theory [25], in order to determine the steady-state heating temperature, T_s :

$$I^2 R_{f(T_s)}{}' dx = hA(T_s - T_a) + \sigma \varepsilon A\left({T_s}^4 - {T_a}^4\right) \quad (4)$$

$$A = 2(w + t_f)dx \quad (5)$$

where h is the convection coefficient of air. $R_{f(T_s)}{}'$ is the electrical resistance per unit length of the carbon fibre tape, which is obtained from experimental measurements discussed above. A is the surface area of the carbon fibre tape and w is the width of the carbon fibre tape. t_f is the thickness of the carbon fibre tape and dx is the length of carbon fibre tape. T_a is the ambient temperature. σ is the Stefan-Boltzmann constant. ε is the emissivity of the carbon fibre tape. I is the current in the electric circuit, which is measured from the static Joule heating test.

As it stands, Equation (4) will overestimate the Joule heating temperature T_s, since the effective surface area of the tape is underestimated in the model. The real cooling area of the carbon fibre tape is larger due to the circular profile of the carbon fibre filaments, compared to the idealised flat rectangular surface. An empirical factor, n, is added to Equation (4) to compensate for that, producing Equation (6). The term n is obtained by fitting the predicted surface temperature from Equation (6) to the steady state temperature obtained from the Joule heating tabletop rig. The prediction shows good agreement with the experimental results when n equals 1.2 and 1.3 for the TX1100 tape and the T700 tow respectively. The difference in n for the two materials is due to the different carbon filament packing arrangement, which yields different microstructures

and surface textures. The filaments within the T700 tows have looser packing patterns; therefore, a larger correction factor is required. It is difficult to calculate the effective surface area accurately due to the heterogeneous properties of the carbon fibre tapes. Materials with similar packing patterns/microstructures are expected to share similar values for n, but this factor will need to be derived for different tow/tape architectures.

$$I^2 R_{f(T_s)}' dx = hnA(T_s - T_a) + \sigma\varepsilon nA\left({T_s}^4 - {T_a}^4\right) \quad (6)$$

3.3 Transient Joule heating model without fibre movement

Two Joule heating experiments using stepped power inputs were conducted on the tabletop rig and the ADFP head. A transient Joule heating model has been built to predict the temperature history in the two experiments. The transient model is presented in equation (7):

$$\frac{\rho C_{p(T)}}{k}\frac{\partial T}{\partial t} = \frac{\partial^2 T}{\partial x^2} + \frac{\dot{q}_{jh}}{k} - \frac{\dot{q}_{con}}{k} - \frac{\dot{q}_{rad}}{k} - \frac{\dot{q}_r}{k} \quad (7)$$

where T is the temperature of the carbon fibre tape. ρ is the density of the carbon fibre tape. $c_{p(T)}$ is the specific heat capacity of the carbon fibre tape. k is the thermal conductivity along the fibre direction of the carbon fibre tape. $\dot{q}_{jh}$, $\dot{q}_{con}$, $\dot{q}_{rad}$ and $\dot{q}_r$ are the volumetric heat generated or dissipated by Joule heating, air convection, radiation and heat loss to the compaction roller respectively, which can be calculated by Equations (8) to (11).

The conductive heat transfer to the compaction roller is modelled as a convective heat transfer with a coefficient of h_c for simplicity. The value of h_c ranges from 200 to 1500 W/(m^{2}K) [26-28] for different tape materials and roller materials. In this research, the value of h_c is obtained by fitting the predicted surface temperature from Equation (7) to the temperature obtained from the ADFP rig, whilst the head is stationary.

$$\dot{q}_{jh} = \frac{I^2 R_{f(T)}' dx}{V} \quad (8)$$

$$\dot{q}_{con} = \begin{cases} \frac{hnA(T-T_a)}{2V} & \text{in ADFP head} \\ \frac{hnA(T-T_a)}{V} & \text{in tabletop rig} \end{cases} \quad (9)$$

$$\dot{q}_{rad} = \begin{cases} \frac{\sigma\varepsilon nA(T^4-{T_a}^4)}{2V} & \text{in ADFP head} \\ \frac{\sigma\varepsilon nA(T^4-{T_a}^4)}{V} & \text{in tabletop rig} \end{cases} \quad (10)$$

$$\dot{q}_r = \begin{cases} \frac{h_c nA_r(T-T_r)}{V} & \text{in ADFP head} \\ 0 & \text{in tabletop rig} \end{cases} \quad (11)$$

$$A_r = wdx \quad (12)$$

$$V = wdxt_f \quad (13)$$

where T_r is the temperature of the rubber skin contacting the carbon fibre tape. V is the volume of the model region.

An explicit finite-difference scheme is used to solve Equation (7). The discretisation of time is shown in Equations (14) and (15):

$$t = p\Delta t \quad (14)$$

$$\frac{\partial T}{\partial t} = \frac{T^{p+1}-T^p}{\Delta t} \quad (15)$$

where t is the total time, Δt is the time interval and p is the integer to denote the time dependence of T.

It is assumed that the carbon fibre tape has uniform temperature along fibre direction and there is no conduction heat transfer within the tape for stationary heating tests in the tabletop rig or the ADFP head. Therefore, Equation (7) can be simplified as:

$$\rho C_{p(T)} \frac{T^{p+1}-T^p}{\Delta t} = \dot{q}_{jh} - \dot{q}_{con} - \dot{q}_{rad} - \dot{q}_r \quad (16)$$

The rubber skin on the compaction roller contacting the carbon fibre tape is modelled as a rectangular block with the same width w, and the same length, dx as the carbon fibre tape, with a thickness of t_r. The temperature of the rubber skin can be calculated using the following equations.

$$\rho_r C_{pr} \frac{T_r^{p+1} - T_r^p}{\Delta t} = \dot{q}_{r1} - \dot{q}_{rc} \quad (17)$$

$$\dot{q}_{r1} = \frac{h_c n A_r (T - T_r)}{V_r} \quad (18)$$

$$\dot{q}_{rc} = \frac{h_r (T_r^p - T_a) A_{rc}}{V_r} \quad (19)$$

$$A_{rc} = 2(w + dx)t_r \quad (20)$$

$$V_r = wdxt_r \quad (21)$$

where ρ_r is the density and C_{pr} is the specific heat capacity of the rubber skin. $\dot{q}_{rc}$ represents the conductive heat transfer to the surrounding rubber materials. It is modelled as a convective boundary condition with a coefficient h_r for simplicity. A_r is the contact area to the surrounding rubber materials. The temperature of the surrounding rubber materials is modelled as a constant ambient temperature T_a.

3.4 Fibre deposition Joule heating model

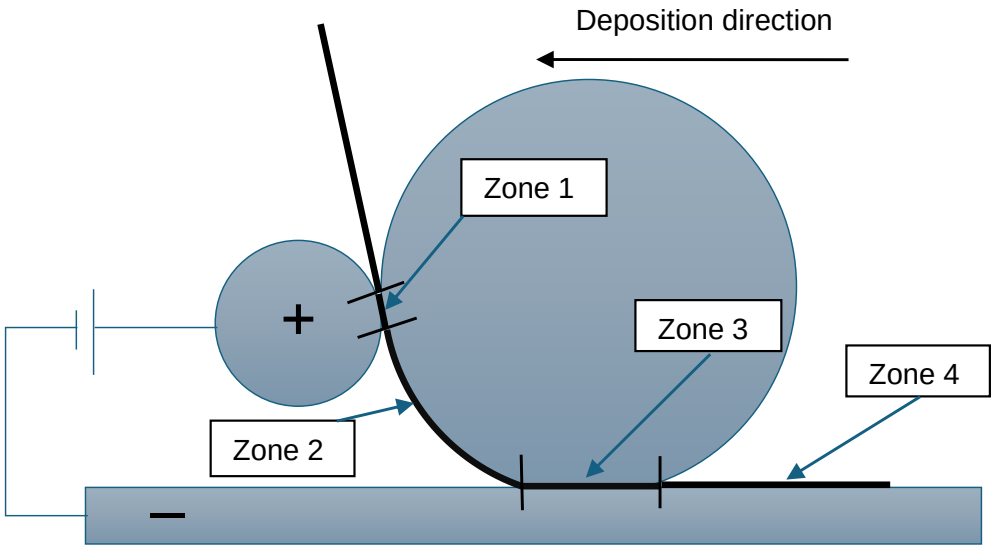

Figure 7 Sketch of Joule heating setup in the lab scale ADFP head

Figure 7 shows the Joule heating process for carbon fibre tapes during the ADFP deposition process. The carbon fibre tape passes through four zones at a defined velocity. In Zone 1, the carbon tape makes contact with the copper electrode and the compaction roller. The contact resistance between the electrode and carbon fibre tape leads to the carbon fibre tape being heated. There is heat loss at this point to the compaction roller. In Zone 2, the carbon fibre tape is under Joule heating by its own electrical resistance. There are convective heat losses and radiative heat losses on the surface exposed to the surrounding air and conductive heat loss to the compaction roller

on the opposite surface. In Zone 3, the carbon fibre tape makes contact with the conductive substrate. The tape is heated by contact resistance heating. There are conductive heat losses to the substrate and to the compaction roller. For Zone 4, the carbon fibre tape is outside of the electrical circuit and is cooling. There are convective heat losses and radiative heat losses on the surface exposed to the air and conductive heat losses to the substrate on the other surface. Heat transfer analyses in Zones 1 and 2 are conducted in this paper, using an analytical model to simulate the temperature in these zones. The nip point temperature is predicted by the model at the end of Zone 2 before contacting the substrate.

A steady-mass-flow method is used to simulate the movement of the carbon fibre, where the rate of mass flow into a control volume is equal to the rate of mass flow out of the control volume. The energy balance in the control volume is presented by Equation (22) [25]:

$$\dot{Q} = \dot{m}\, C_{p(T)} \Delta T \tag{22}$$

$$\Delta T = T_2 - T_1 \tag{23}$$

$$\dot{m} = \rho v A_c \tag{24}$$

$$A_c = w t_1 \tag{25}$$

where $\dot{Q}$ is the net heat transfer into or out of the control volume, $\dot{m}$ is the mass flow rate, ΔT is the temperature difference between the inlet T_1 and outlet T_2 of the control volume, v is the deposition velocity and A_c is the cross-section area of the carbon fibre tapes. The length of the control volume in this model is 0.2 mm.

Using this method, the outlet temperature T_2 can be calculated if the inlet temperature T_1 and net heat transfer $\dot{Q}$ are known. Various control volumes are connected in series to form the length of the model. The outlet temperature T_2 of the first control volume is used as the inlet temperature T_1 of the next control volume. The conduction heat transfer between the control volumes is negligible. The temperature at the inlet of the first control volume is assumed to be ambient temperature T_a, at 25 °C.

It is assumed that half of the energy from the contact resistance heating is used to heat the carbon fibre tapes in Zone 1. The length of Zone 1 is 1 mm and five control volumes are connected in series. Both outlet carbon fibre tape temperature T_2 and compaction roller temperature T_{r2} are calculated using the following equations:

$$\frac{I^2 R_{c(v)}{}' dx}{2} - h_c(T_1 - T_{r1})A_r = \rho v A_c C_{p(T)}(T_2 - T_1) \tag{26}$$

$$-h_r(T_{r1} - T_a)A_{rc} - h_c(T_{r1} - T_1)A_r = \rho_r v A_{cr} C_{pr}(T_{r2} - T_{r1}) \tag{27}$$

$$A_{cr} = wt_r \tag{28}$$

where $R_{c(v)}{}'$ is the contact resistance per unit length in Zone 1. It was found that the contact resistance between the carbon fibre tape and copper cylinder electrode increases with the increase of fibre feeding velocity [14]. In this model, a linear relationship between contact resistance $R_{c(v)}{}'$ and deposition velocity v is used. $R_{c(v)}{}'$ is independent of temperature for simplicity.

The length of Zone 2 is 54 mm and 270 control volumes are connected in series after the five control volumes in Zone 1. The following equation is used to calculate the outlet temperature of the carbon fibre tape of the control volumes in Zone 2. Equation (28) is used for the roller outlet temperature calculations.

$$I^2 R_{f(T)}{}' dx - h_c(T_1 - T_r)A_r - hn\frac{A}{2}(T_1 - T_a) - \sigma\varepsilon n\frac{A}{2}({T_1}^4 - {T_a}^4) = \rho v A_c C_{p(T)}(T_2 - T_1) \tag{29}$$

Table 2 summarises all of the parameters used in the models above.

Table 2 Model parameters

Input	Symbol	Units	TX1100	T700
Deposition velocity	v	mm/s	10, 25, 50, 100	-
Contact resistance per unit length between copper electrode and TX1100 tape	$R_{c(v)}{}'$	Ω/mm	(0.0089 v + 0.11) §	-
Tape density	ρ	kg/m^3	785*	872*
Control volume/model length	dx	mm	0.2	
Tape width	w	mm	6.35†	
Tape thickness	t_f	mm	0.27*	0.15*
Tape resistance per unit length (taken from Figure 9 (a))	$R_{f(T)}{}'$	Ω/m	(-0.0078 T + 22.65)*	(-0.0228 T + 37.13)*
Tape specific heat capacity (taken from Figure 1)	$C_{p(T)}$	J/(kg°C)	(2.6704 T + 1033.7)*	(2.2969 T + 554.05)*
Coefficient of heat loss from tape to compaction roller	h_c	W/(m^{2}K)	230	
Roller rubber skin density	ρ_r	kg/m^3	1080†	

Roller rubber skin specific heat capacity	C_{pr}	J/(kg°C)	1050 [29, 30]	
Skin thickness – Rubber roller	t_r	mm	3	
Coefficient of heat loss from roller to surrounding materials	h_r	W/(m^{2}K)	3 §	
Correction factor for the surface area of CF tapes	n	-	1.2	1.3
Convective coefficient of air	h	W/(m^{2}K)	12.12 [25]	
Emissivity	ε	-	0.85 [3, 31]	
Ambient temperature	T_a	°C	25	
Time interval	Δt	s	0.001	
Stefan-Boltzmann constant	σ	Wm^{-2}K^{-4}	5.67×10^{-8}	

* Measured or derived from experiments

† From manufacturer's datasheet

§ Estimated value

4 Results and Discussion

4.1 Effect of wrap angle and fibre tension on contact resistance

Figure 8 (a) shows values for the contact resistance of the TX1100 tape at room temperature, with the binder surface facing the electrode, under different contact angles and fibre tensions. For all contact angles, the contact resistance reduces significantly with increasing fibre tension before reaching a plateau value. Increasing fibre tension increases the number of filaments in contact with the electrodes and therefore the effective filament contact area, which decreases the contact resistance [16]. Increasing fibre tension can only reduce the contact resistance so far before the plateau value is reached, since further increases in tension do not change the distribution of filaments within the tape. Increasing contact angle can also lead to a reduction in contact resistance, particularly at low tension levels, since the contact area is greater with higher contact angles. However, the tape contact angle with the electrode is limited by the deposition hardware, therefore increasing tape tension is a more practical way to reduce contact resistance.

Figure 8 (b) shows the contact resistance results for the T700 tows. The contact resistance values of T700 tows are larger than those of the TX1100 tapes (except the

case of 100 N fibre tension with 31.0°). TX1100 tapes have carbon fibres with smaller diameters (5 μm compared with 7 μm), therefore more fibres make contact with the electrodes than for the T700 tows, which leads to a lower contact resistance. The binder on the surface of TX1100 tapes has less influence on the contact resistance because only a small area is covered by the binder. The influence of fibre tension and wrap angle is similar for both materials.

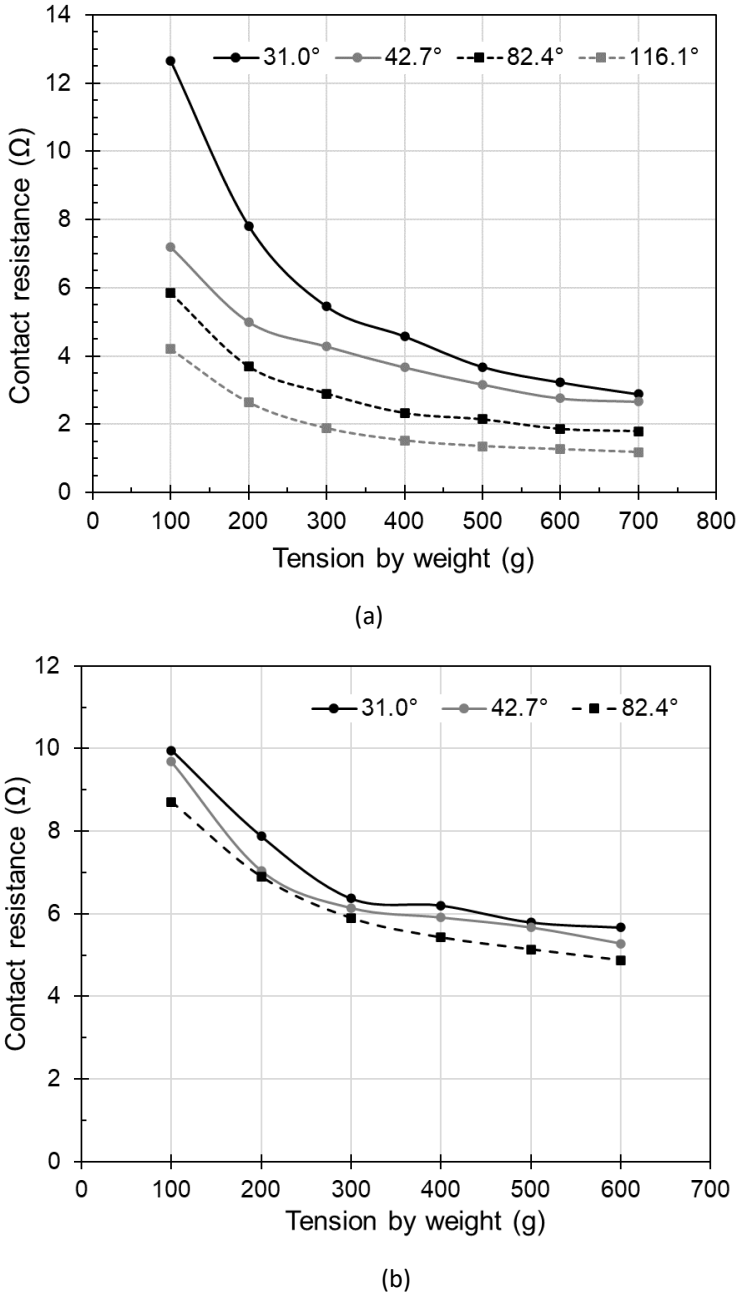

Figure 8 Contact resistance measurement results for (a) TX1100 tape (binder surfaces facing electrode) (b)T700 tow under different fibre tension and wrap angle at room temperature

4.2 Effect of temperature on electrical resistance and contact resistance

Figure 9 shows the influence of temperature on the electrical resistance and contact resistance. The electrical resistance decreases linearly for both materials with increasing temperature, which agrees with data from the literature [22, 23]. The contact resistance also decreases with increasing temperature for both materials, this has been suggested [16] to be due to an increasing contact area caused by the transverse thermal expansion of the carbon filaments. T700 tows generally have a lower contact resistance than the TX1100 tapes at elevated temperatures.

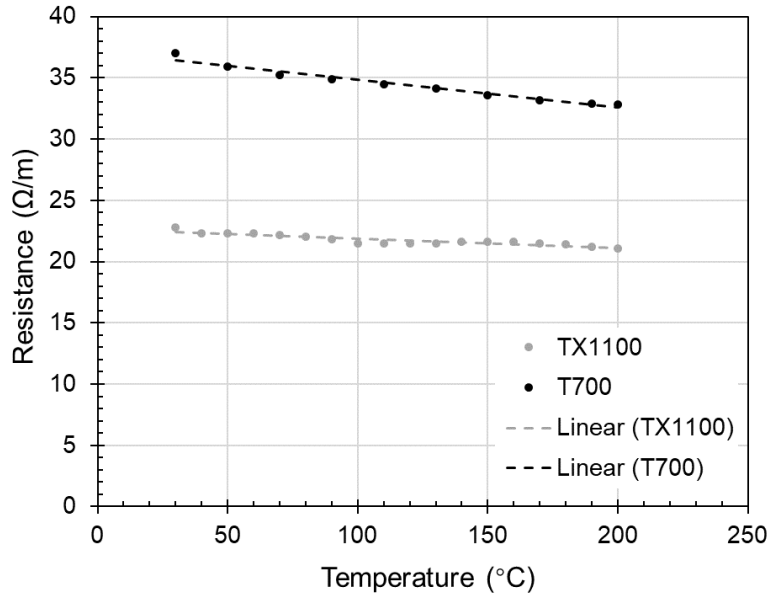

(a)

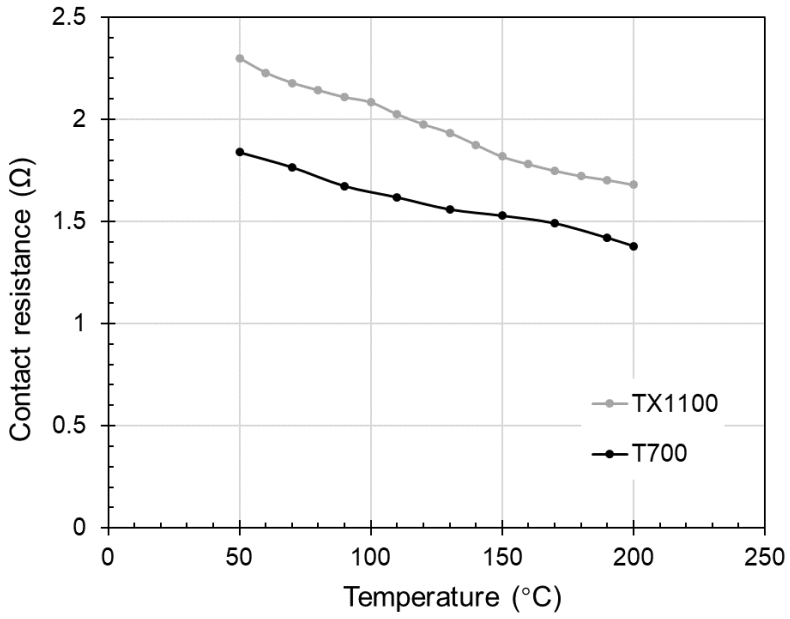

(b)

Figure 9 (a) Electrical resistance (b) contact resistance results of TX1100 tape and T700 tow under different heating temperature with a wrap angle of 82.4° and a fibre tension of 300 g

4.3 Joule heating efficiency

Figure 10 shows the Joule heating efficiency results calculated by Equation (3), using the experimental contact resistance at room temperature. It is clear that increasing fibre tension leads to an increase in heating efficiency due to lower contact resistance. Longer tape lengths also lead to higher efficiency, due to their higher electrical resistance. Under low fibre tension (less than 300 g), T700 tows have higher heating efficiency while under high fibre tension (more than 300 g), TX1100 tapes have higher heating efficiency. It is recommended that the length of the heating region in the deposition head is maximised to reduce the energy consumed in the contact region. Heating efficiency is somewhat dependent on temperature, but this effect is not significant as shown in Figure 11. Whilst contact resistance decreases with the increase in temperature, the resistance of the tapes also decreases. The nominal heating efficiency increases by less than 10 % as the temperature increases from 50 °C to 200 °C.

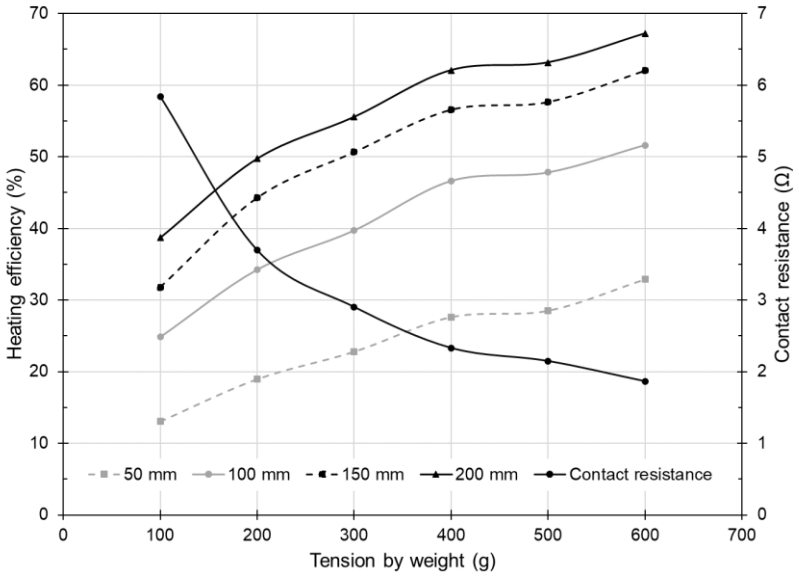

(a)

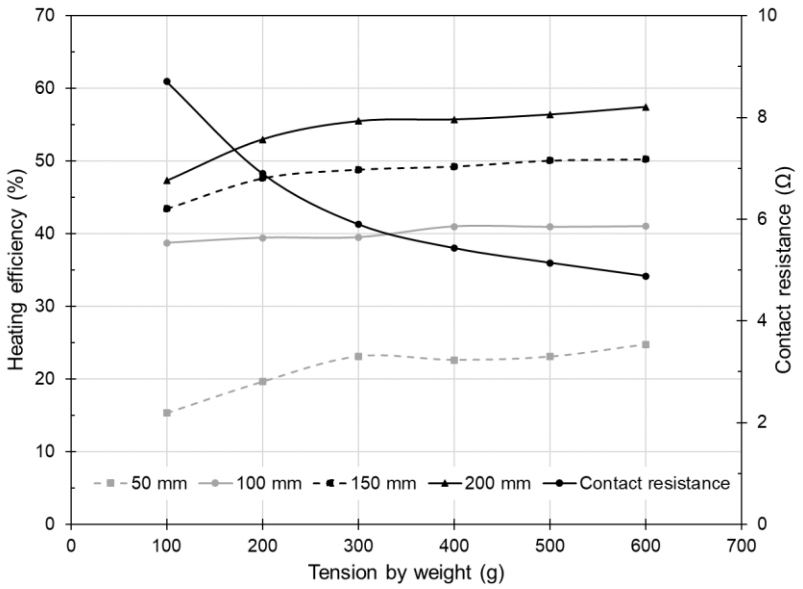

(b)

Figure 10 Joule heating efficiency of (a) TX1100 tape (b) T700 tow at wrap angle of 82.4 ° under four heating length at room temperature

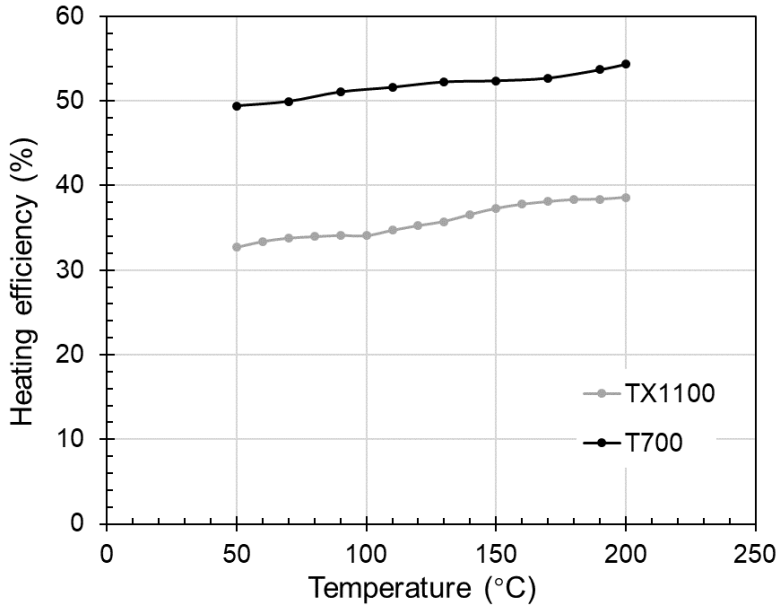

Figure 11 Joule heating efficiency of two materials at different temperatures at wrap angle of 82.4 ° under 50 mm heating length

4.4 Joule heating - Tabletop rig

Figure 12 shows temperature values measured during steady-state Joule heating experiments for the two materials, compared with predictions from Equation (6). The steady-state temperature increases linearly above values of 75 °C, which agrees with the findings by Athanasopoulos et al [22]. For the same current input values, T700 tows exhibit higher steady-state temperatures compared to TX1100, due to their higher

electrical resistance. The analytical model agrees well with the experimental results. The error is less than 5 % in both cases, confirming the validity of Equation (6).

Figure 13 shows the heating and cooling curves for the two materials during a 30 second heating period using the tabletop rig. The predicted temperature values agree well with the surface temperatures measured from the experiments. The errors are less than 11 % in each case, confirming the validity of the transient terms used in the model.

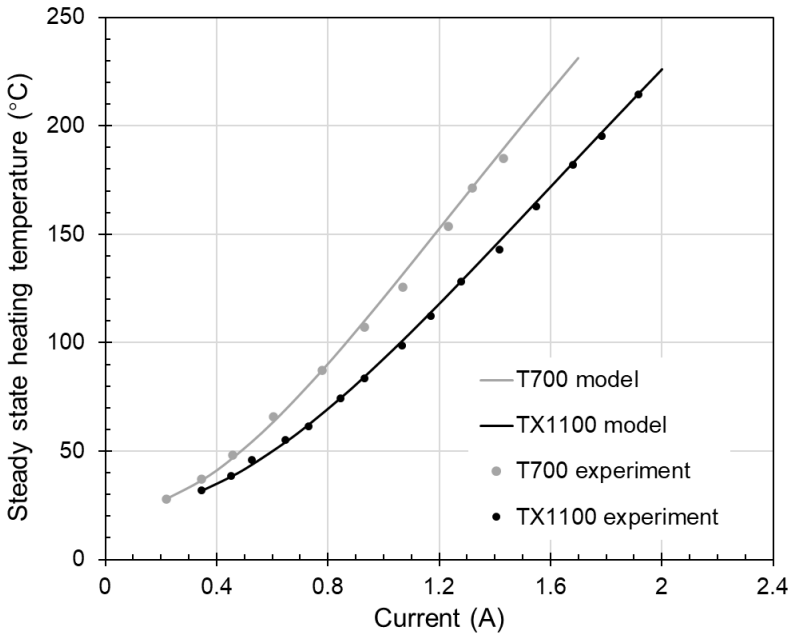

Figure 12 Steady state heating temperature with wrap angle of 82.4 ° and fibre tension of 300 g, for a heating length of 50 mm

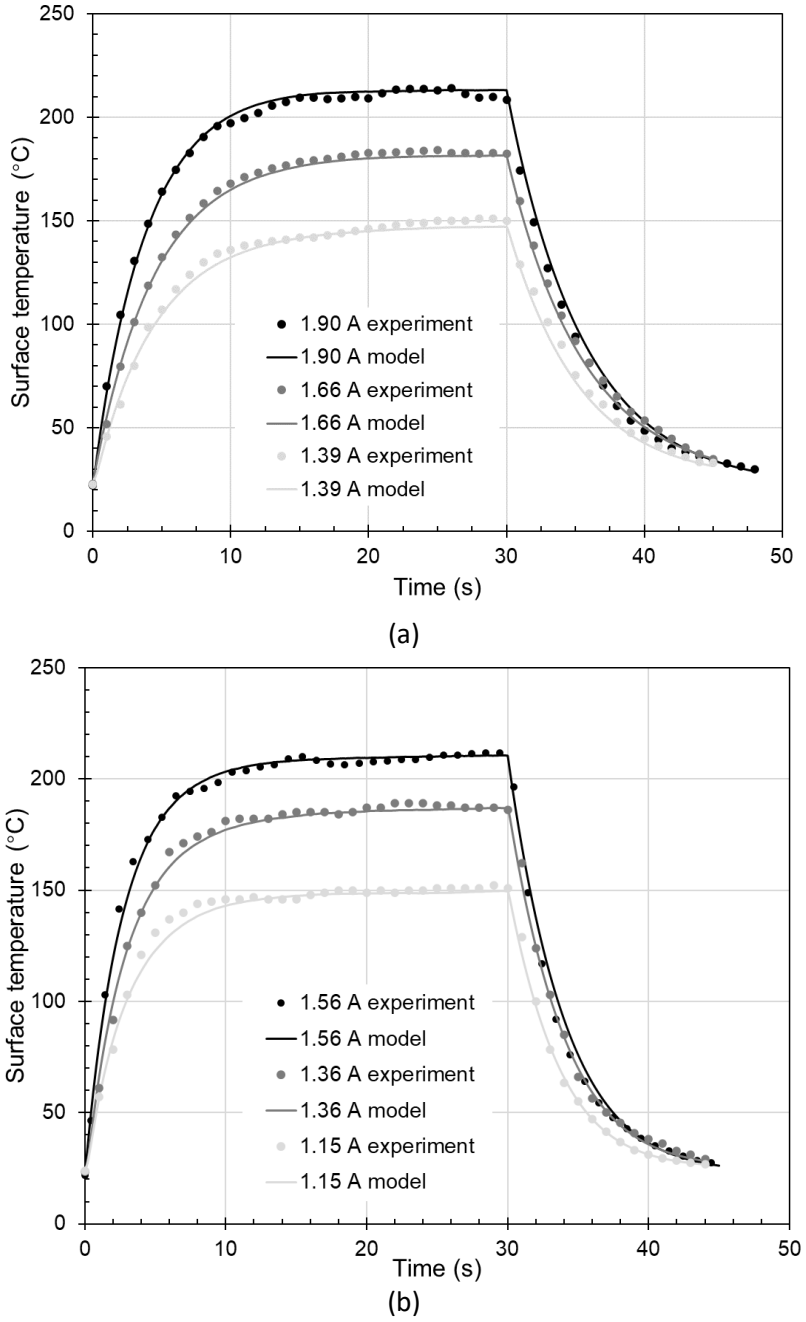

Figure 13 Joule heating results from the tabletop rig for a 30 s heating time and different electrical current set points. (Tow/tape heating length of 100 mm, wrap angle of 82.4 ° and fibre tension of 300 g) (a) TX1100 (b) T700

4.5 Joule heating - ADFP deposition head

Figure 14 shows the results of Joule heating trials using a static tape in the ADFP head. The model predicts the change in temperature adequately, with a maximum error value of 10% compared to the experimental data. This study confirms the validity of the term used in the model to account for the heat loss to the compaction roller.

Figure 15 shows the experimental results and model predictions for dynamic Joule heating tests, using four different fibre deposition velocities. The temperature of the

fibre at a distance of 15 mm beyond the copper electrode (see Figure 6 for measurement location) increases almost linearly with the increase of applied current for all deposition velocities. In general, higher currents are required to reach the same target temperature when depositing at higher velocities. The errors for the linear predictions are generally within 13 % compared to the experimental data.

The model can be used to predict the nip point heating temperature (temperature at the end of Zone 2) as shown in Figure 16. The activation temperature of TX1100 is around 160 °C [32]. It is found that the nip point heating temperature increases linearly with the increase of applied current for all deposition velocities. The gradient of the curve decreases with increasing deposition velocity, indicating that higher input currents are required to achieve the same nip point temperature for higher deposition velocities.

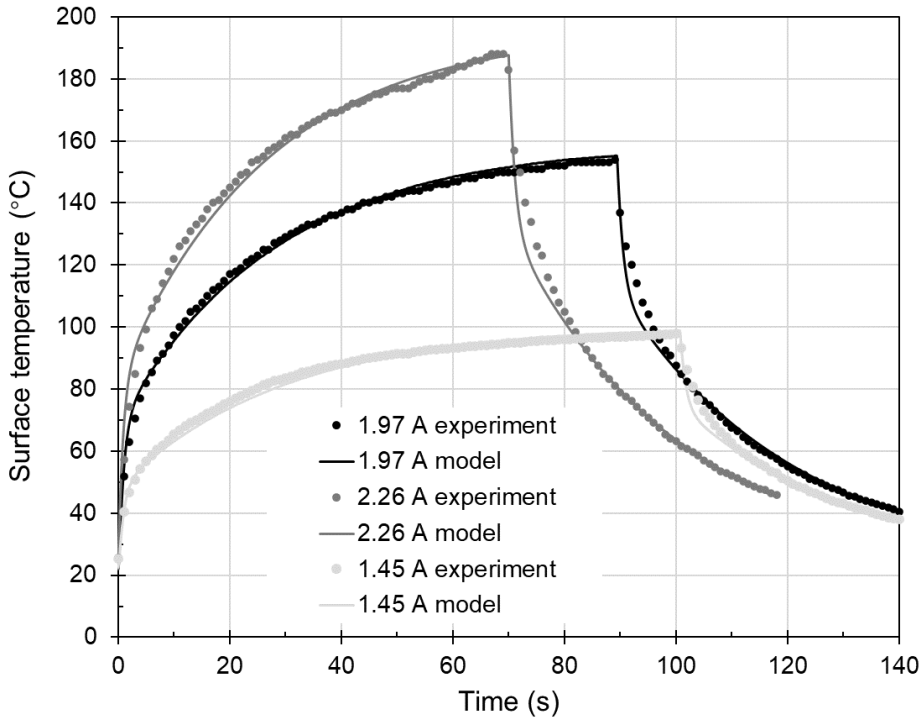

Figure 14 Joule heating test results from the stationary ADFP head for TX1100 tape at three applied electrical current values.

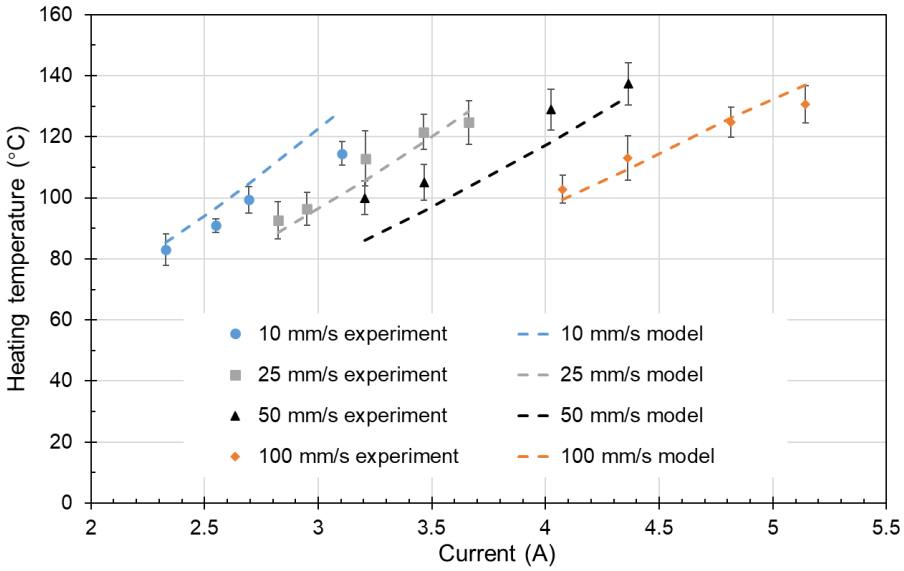

Figure 15 Joule heating with fibre deposition tests results (The heating temperature is at 15 mm after the copper electrode. Error bars show the standard deviation of measured temperature along the deposition length.)

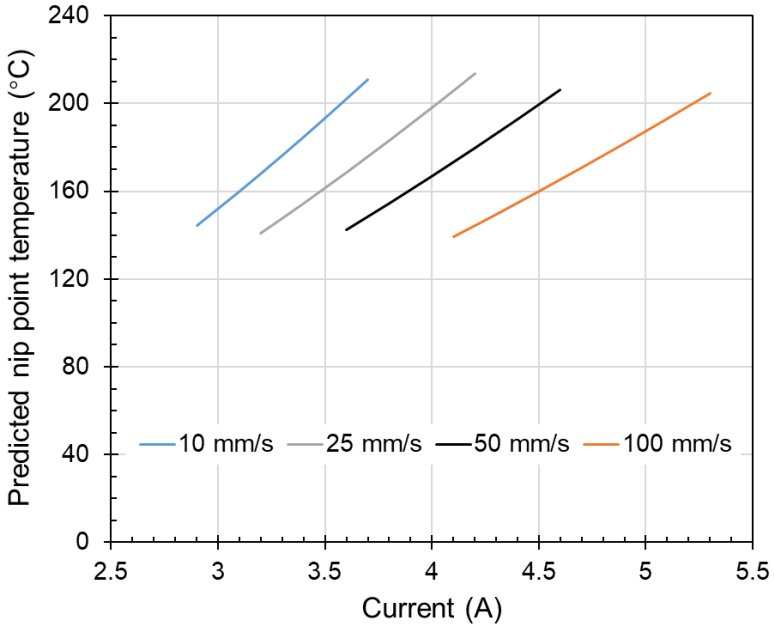

Figure 16 Predicted nip point temperature for different deposition velocities

4.6 Joule heating energy consumption

Figure 17 shows the relationship between nip point temperature and the required power consumption using Joule heating and laser heating for TX1100 tapes at a deposition velocity of 100 mm/s. Power consumption for Joule heating is calculated from the power supply voltage and current value measured by the shunt resistor. The nip point temperature is predicted by the developed model. Di Francesco et al [3] obtained the relationship between the laser power output and the measured nip point temperature of TX1100 tape. According to the manufacturer's data sheet [33] for the

fibre-coupled diode laser used by Di Francesco [3], the total power consumption is about four times the output power of the laser, producing the dotted black line in Figure 17. The nip point temperature increases linearly with increasing power for both Joule heating and laser heating. Laser heating consumes approximately 20% more energy than Joule heating for a nip point temperature of 200 °C. The energy saving for Joule heating is not as high as expected for this set up, as the contact length between the carbon fibre tapes and the compaction roller is quite high before reaching the nip point. The contact length of 55 mm for the current ADFP machine is approximately five times higher than the AFP setups in the literature (around 10 mm [28, 34]). The energy losses to the compaction roller are also significant, constituting around 90 % of the total energy losses when the nip point temperature is around 200 °C. In addition to the lower power consumption for Joule heating, the main advantage is the lower hardware costs, which are at least 30 % lower than that of a comparable laser or flashlamp setup [19]. Joule heating for ADFP uses extra low voltage (ELV), which greatly reduces the risk of electric shock. Furthermore, no special safety measures are required for Joule heating, unlike laser heating [19]. However, material choice is limited for Joule heating, as the fibres must be conductive, and there are questions over temperature uniformity, particularly at the tape edges.

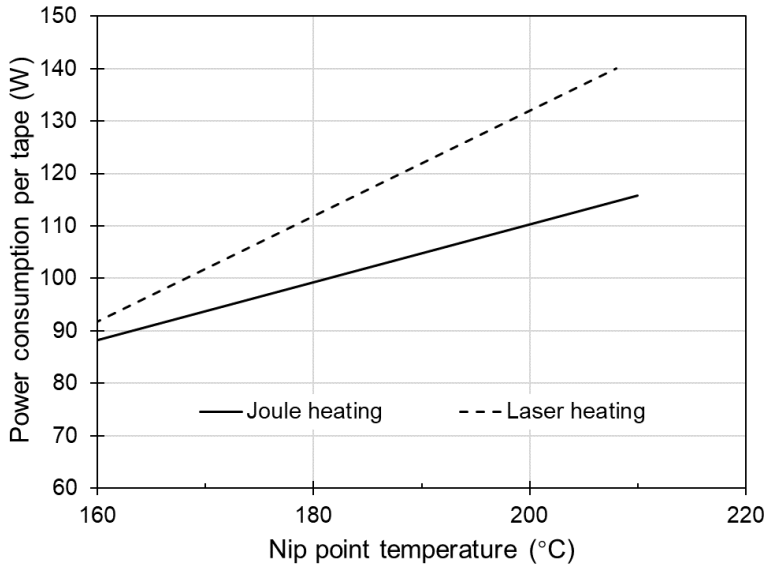

Figure 17 Power consumption of Joule heating and laser heating of TX1100 tapes at a deposition velocity of 100 mm/s (Laser heating energy consumption is reproduced from [3])

5 Conclusions

In this paper, the electrical properties of carbon fibre tapes and the contact resistance between the electrodes and carbon fibre tapes have been characterised. The Joule heating method has been successfully implemented using a laboratory scale ADFP deposition head. Analytical models have been built and validated to predict the nip point heating temperature during the ADFP process, under different deposition velocities and different current inputs. The models are helpful for better Joule heating temperature control on the deposition head.

The contact resistance between the carbon fibre tapes and the cylindrical copper electrodes (at low levels of fibre tension) is of the same order of magnitude as the electrical resistance of the carbon fibre tapes. This results in low heating efficiency and therefore low tape temperatures. Increasing fibre tension and wrap angle can reduce the contact resistance, increasing the efficiency of the Joule heating process by up to 30%. Both the electrical resistance of carbon fibre tapes and the contact resistance decrease with increase temperature. The efficiency of the Joule heating process increases by less than 10%, as the temperature increases from 50 °C to 200 °C.

The predictions from the analytical Joule heating model during fibre deposition show good agreement with the experimental temperature measurement. It can be shown from the model predictions that the nip point temperature increases linearly with the increase of applied current at all deposition velocities. For higher deposition velocities, higher currents are needed to increase the nip point temperature.

Energy consumption using Joule heating in ADFP increases linearly with the increase of nip point heating temperature, which is the same as for laser heating when processing the same material. However, the Joule heating method developed in this paper only consumes 83 % of the energy used during laser heating to produce a nip point temperature of 200 °C at a deposition velocity of 100 mm/s.

6 Acknowledgements

This work was supported by the Engineering and Physical Sciences Research Council [grant number EP/P006701/1], as part of the EPSRC Future Composites Manufacturing

Research Hub, and as part of the Made Smarter Innovation - Materials Made Smarter Research Centre [grant number EP/V061798/1].

7 References

[1] Potter K. 6 - Automated fibre placement. In: Harper L, Clifford M, editors. Design and Manufacture of Structural Composites: Woodhead Publishing; 2023. p. 125-43.
[2] Assadi M, Field T. AFP Processing of Dry Fiber Carbon Materials (DFP) for Improved Rates and Reliability. SAE Technical Paper Series2020.
[3] Di Francesco M, Veldenz L, Dell'Anno G, Potter K. Heater power control for multi-material, variable speed Automated Fibre Placement. Composites Part A: Applied Science and Manufacturing. 2017;101:408-21.
[4] Liu YN, Yuan C, Liu C, Pan J, Dong Q. Study on the resin infusion process based on automated fiber placement fabricated dry fiber preform. Sci Rep. 2019;9(1):7440.
[5] Kadiyala AK, Portela A, Devlin K, Lee S, O'Carroll A, Jones D, et al. Mechanical evaluation and failure analysis of composite laminates manufactured using automated dry fibre tape placement followed by liquid resin infusion. Composites Science and Technology. 2021;201.
[6] Ehsani F, Hoa SV, Shadmehri F. Effect of gaps on preform and laminate made by automated dry fiber placement and resin infusion. Composites Part A: Applied Science and Manufacturing. 2023;173.
[7] Brasington A, Sacco C, Halbritter J, Wehbe R, Harik R. Automated fiber placement: A review of history, current technologies, and future paths forward. Composites Part C: Open Access. 2021;6.
[8] Monnot P, Williams D. Power control of a flashlamp-based heating solution for automated dry fibre placement. 18th European Conference on Composite Materials, ECCM18. Athens, Greece2018.
[9] Deden D, Bruckner F, Brandt L, Fischer F. Comparison of heat sources for automated dry fibre placement: Xenon flashlamp vs. infrared heating. 22nd International Conference on Composite Materials (ICCM22). Melbourne2019.
[10] Martins RdA. Joule's 1840 manuscript on the production of heat by voltaic electricity. Notes and Records: the Royal Society Journal of the History of Science. 2022;76(1):117-54.
[11] Yue C, Zhang Y, Lu W, Zhang Y, Wang P, Li Y, et al. Realizing the curing of polymer composite materials by using electrical resistance heating: A review. Composites Part A: Applied Science and Manufacturing. 2022;163.
[12] Collinson MG, Swait TJ, Bower MP, Nuhiji B, Hayes SA. Development and implementation of direct electric cure of plain weave CFRP composites for aerospace. Composites Part A: Applied Science and Manufacturing. 2023;172.
[13] Brassard D, Dubé M, Tavares JR. Resistance welding of thermoplastic composites with a nanocomposite heating element. Composites Part B: Engineering. 2019;165:779-84.
[14] Stavrov D, Bersee HEN. Resistance welding of thermoplastic composites-an overview. Composites Part A: Applied Science and Manufacturing. 2005;36(1):39-54.
[15] Çelik M, Maguire JM, Noble T, Robert C, Ó Brádaigh CM. Numerical and experimental investigation of Joule heating in a carbon fibre powder epoxy towpregging line. Composites Part A: Applied Science and Manufacturing. 2023;164.
[16] Çelik M, Noble T, Haseeb A, Maguire J, Robert C, Ó Brádaigh CM. Contact resistance heating of unidirectional carbon fibre tows in a powder-epoxy towpregging line. Plastics, Rubber and Composites. 2022;51(8):383-92.
[17] Guo X, Yang Q, Zheng H, Dong W. Integrated composite electrothermal de-icing system based on ultra-thin flexible heating film. Applied Thermal Engineering. 2024;236.

[18] Rohani H, Woo PC. The resistive heating, defrosting, and thermal performance of CFRPs as a heat transfer unit in a frozen environment. International Communications in Heat and Mass Transfer. 2023;147.
[19] Grohmann Y. Continuous resistance heating technology – risks and opportunities of a novel heating method. 20th European Conference on Composite Materials, ECCM20. Lausanne, Switzerland2022.
[20] Helber F, Amann A, Carosella S, Middendorf P. Intrinsic fibre heating: a novel approach for automated dry fibre placement. IOP Conf Ser: Mater Sci Eng: IOP Publishing; 2018. p. 12064.
[21] Grohmann Y. CoRe HeaT - A new heating method for faster fibre placement. ICMAC 2018 - 11th International Conference on Manufacturing of Advanced Composites. England2018.
[22] Athanasopoulos N, Sikoutris D, Panidis T, Kostopoulos V. Numerical investigation and experimental verification of the Joule heating effect of polyacrylonitrile-based carbon fiber tows under high vacuum conditions. Journal of Composite Materials. 2011;46(18):2153-65.
[23] Grohmann Y. Continuous resistance heating technology for high-speed carbon fibre placement processes SAMPE Europe Conference 2020 Amsterdam2020.
[24] Veldenz L, Di Francesco M, Giddings P, Kim BC, Potter K. Material selection for automated dry fiber placement using the analytical hierarchy process. Advanced Manufacturing: Polymer & Composites Science. 2019;4(4):83-96.
[25] Cengel Y. Heat Transfer: A Practical Approach: McGraw-Hill Education; 2004.
[26] Kollmannsberger A, Lichtinger R, Hohenester F, Ebel C, Drechsler K. Numerical analysis of the temperature profile during the laser-assisted automated fiber placement of CFRP tapes with thermoplastic matrix. Journal of Thermoplastic Composite Materials. 2017;31(12):1563-86.
[27] Stokes-Griffin CM, Compston P, Matuszyk TI, Cardew-Hall MJ. Thermal modelling of the laser-assisted thermoplastic tape placement process. Journal of Thermoplastic Composite Materials. 2013;28(10):1445-62.
[28] Barzegar A, Karimi S, Sukur EF, Sas HS, Yildiz M. Effect of fiber orientation on temperature history during laser-assisted thermoplastic fiber placement. Journal of Reinforced Plastics and Composites. 2022.
[29] Liu X, Han Z, Zhao Z, Sun S. Thermal analysis of cylindrical molds using thermoplastic composite during robotic fiber placement. Journal of Physics: Conference Series: IOP Publishing; 2021. p. 012023.
[30] Blinzler BJ, Khalili P, Ahlstrom J. Integrated Computational Material Design for PMC Manufacturing with Trapped Rubber. Materials (Basel). 2020;13(17).
[31] Druiff PP, Monnot P, DellAnno G, Di Francesco M, Ward C. Effective Emissivity Characterisation and Correction for Accurate Control of Automated Fibre Placement Processes. Society for the Advancement of Material and Process Engineering Europe Conference and Exhibition 20202020.
[32] Di Francesco M. Laser-assisted Automated Fibre Placement Process Development [EngD Thesis]: University of Bristol; 2017.
[33] Laserline LDM. The compact classfor diode laser. https://www.laserlines.co.uk/wp-content/uploads/2018/08/Laserline_LDM_The_Compact_Class_for_Diode_Lasers.pdf (accessed 31 July 2024).
[34] Cao Z, Dong M, Liu K, Fu H. Temperature Field in the Heat Transfer Process of PEEK Thermoplastic Composite Fiber Placement. Materials (Basel). 2020;13(19).